ACS NANO

www.acsnano.org

ARTICLE

Tuning Chirality of Self-Assembled PTCDA Molecules on a Au(111) Surface by Na Coordination

Zhewen Liang, Shiru Wu, Jiamin Wang, Yifan Qin, Fang Cheng, Liang Cao,* and Hai Xu*

Cite This: *ACS Nano* 2023, 17, 10938−10946

Read Online

ACCESS | Metrics & More | Article Recommendations | Supporting Information

ABSTRACT: Chiral nanostructures are much desired in many applications, such as chiral sensing, chiroptics, chiral electronics, and asymmetric catalysis. In building chiral nanostructures, the on-surface metal−organic self-assembly is naturally suitable in obtaining atomically precise structures, but that is under the premise that there are enantioselective assembly strategies to create large-scale homochiral networks. Here, we report an approach to build chiral metal−organic networks using 3,4,9,10-perylene tetracarboxylic dianhydride (PTCDA) molecules and low-cost sodium chloride (NaCl) in a controllable manner on Au(111). The chirality induction and transfer processes during network evolution with increased Na ion ratios were captured by scanning tunneling microscopy (STM), X-ray photoelectron spectroscopy (XPS), and density functional theory (DFT) methodologies. Our findings show that Na ion incorporation into achiral PTCDA molecules partially breaks intermolecular hydrogen bonds and coordinates with carboxyl oxygen atoms, which initiates a collective sliding motion of PTCDA molecules along specific directions. Consequently, "molecular columns" linked by hydrogen bonds were formed in the rearranged Na-PTCDA networks. Notably, the direction of Na ion incorporation determines the chiral characteristic by guiding the sliding direction of the molecular columns, and chirality can be transferred from $Na_{0.5}$PTCDA to Na_1PTCDA networks. Furthermore, our results indicate that the chirality transferring process is disrupted when intermolecular hydrogen bonds are entirely replaced by Na ions at a high Na dopant concentration. Our study provides fundamental insights into the mechanism of coordination-induced chirality in metal−organic self-assemblies and offers potential strategies for synthesizing large homochiral metal−organic networks.

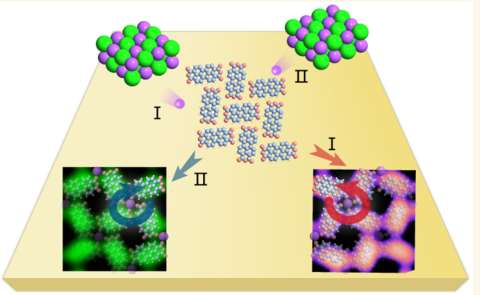

KEYWORDS: *chirality, alkali incorporation, metal−organic coordination, scanning tunneling microscopy, density functional theory (DFT)*

INTRODUCTION

Chiral supramolecular nanostructures are a new class of chiral materials that have potential applications in chiroptics and spintronics.[1−4] Symmetry-breaking processes are fundamental to the design of chiral structures.[5−9] The surface, which provides a symmetry-breaking environment, offers opportunities to construct chiral supramolecular structures using achiral molecules. The breaking of mirror-symmetry occurs spontaneously during molecular adsorption on surfaces owing to the surface constraint. However, sometimes the surface symmetry breaking alone is insufficient to produce chiral supramolecular structures. To further induce symmetry breaking of achiral molecules, a practical approach is to modify the molecular arrangement by modulating the intermolecular interactions.[10−21] For example, metal-coordination interactions can provide additional flexibility in breaking the symmetry, which can serve as a tuning knob to further control the chirality of self-assembled supramolecular structures.[22−26] Moreover, the linking of molecular building blocks by strong metal−organic coordination bonds (also known as reticular chemistry) allows the formation of stable chiral networks with atomically precise structures and hence tailored functionalities.

In order to create large-scale homochiral networks, one should develop effective enantioselective assembly strategies. However, such efforts are often hindered by the lack of understanding of the chirality induction and transfer processes during self-assembly, because of the difficulty in observing the early and intermediate self-assembly stages.[19] The achiral 3,4,9,10-perylene tetracarboxylic dianhydride (PTCDA) mol-

Received: March 28, 2023
Accepted: May 16, 2023
Published: May 25, 2023

ecule is a typical organic semiconductor.[27,28] Doping PTCDA with alkali metals to modulate its electric conductivity was intensively studied in the past, mostly by using alkali metals supplied from the gas phase.[29−36] However, gas-phase alkali deposition often results in a fast coordination process, and therefore the early and intermediate stages of network formation, which are essential in understanding the chirality induction and transfer processes, cannot be captured. Recently, alkali metal salts such as sodium chloride (NaCl) have emerged as a solid-state sodium source.[37,38] The predeposited NaCl domains can be viewed as a sustained-release source of Na ions: by controlling the annealing temperature and annealing time, one can precisely regulate the NaCl decomposition rate and hence the amount of Na ions released for coordination. Meanwhile, the NaCl domains and molecular domains coexist on the surface, leading to the Na-induced coordination process starting from the edge of the molecular domain. This is in stark contrast with the gas-phase Na deposition method, where the coordination process occurs randomly over the entire molecular domain. Therefore, the use of a solid-state alkali source provides a vital degree of freedom to precisely control the enantioselective self-assembly process and observe the evolution of the Na-PTCDA networks in detail (see Scheme 1).

Herein, we present a detailed account of the growth and characterization of Na-PTCDA networks on a Au(111) surface, accompanied by observations of the chirality induction and transfer processes at the single-molecule level using high-resolution scanning tunneling microscopy (STM). Initially, we co-deposited achiral PTCDA domains and NaCl islands on the Au(111) surface. By adjusting the NaCl/PTCDA ratio and annealing temperature, we created a range of chiral Na-PTCDA networks with stoichiometry ranging from $Na_{0.5}$PTCDA to Na_2PTCDA. Density functional theory (DFT) studies revealed that Na ion incorporation into the achiral PTCDA herringbone (HB) lattice partially breaks the intermolecular hydrogen bonds to coordinate with the carboxyl oxygen atoms. The remaining hydrogen bonds and steric interactions lead to the rearrangement of the PTCDA molecule in a collective sliding mode, which plays a crucial role in the induction and transfer of chirality in Na-PTCDA networks. Our STM results show that this collective sliding motion is strongly correlated with the direction of Na ion incorporation in Na-PTCDA networks, which determines the final left- or right-handed characterization in chirality. However, when the Na:PTCDA ratio is increased to 2:1 in the Na_2PTCDA product, the intermolecular hydrogen bonds that facilitate the collective molecular rearrangement are entirely replaced by Na−O coordination bonds, disrupting the chirality transfer process. Our findings will give valuable insights for understanding the induction and transfer of the chirality in metal−organic networks.

Scheme 1. Schematic illustration of Na ion incorporation into the PTCDA domains in two ways: (a) out-of-plane by gas-phase Na ions; (b, c) in-plane with different directions by solid-state Na ions released from co-deposited NaCl.

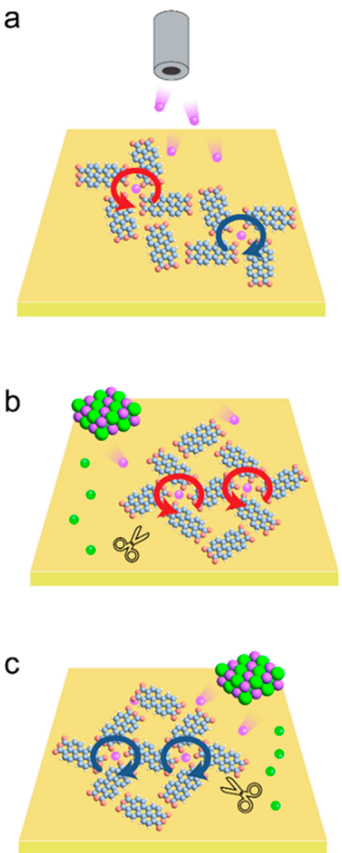

RESULTS AND DISCUSSION

First, we deposited PTCDA (Figure 1a) molecules on the Au(111) surface at room temperature (RT). Figure 1b shows the PTCDA molecules self-assembled into a well-ordered HB structure held by hydrogen bonds.[39] As shown in the STM image of Figure 1c, the flat-lying molecules can be classified into two categories, A and B, depending on their adsorption orientation. Molecule A is approximately parallel to the $[10\bar{1}]$ direction of the Au(111) lattice, while molecule B is tilted by an angle of 77° to it, which is similar to previous reports on PTCDA domains adsorbed on Au(111) and Ag(111).[40,41] Here, the unit cell exhibits a mirror symmetry represented by blue and red dashed boxes, demonstrating that this self-assembled HB structure is achiral. Based on this unit cell, we define the orientation of the PTCDA two-dimensional lattice as shown in Figure 1c.[40] The PTCDA domains do not lift the HB reconstruction of Au(111) as shown in Figure 1b, indicating a relatively weak interaction with the surface.

To precisely control the Na ion coordination with the PTCDA self-assembled domains, we used NaCl as the solid-state Na source. After depositing PTCDA molecules on the Au(111) surface with predeposited NaCl and subsequent annealing at 350 K for 5 min, we observed a PTCDA film formed nearby a small NaCl island (Figure 2a). Compared to Figure 1b, this structure is divided into two phases separated by the white dashed line. A porous structure was formed around the NaCl patch, while most of the film still retained the HB structure. To verify the presence of Na-dopant, we performed X-ray photoelectron spectroscopy (XPS) analysis on the samples with co-deposited PTCDA and NaCl. After successive annealing of the sample, the chemical shift of oxygen core level peaks is consistent with the effect of electron doping by Na dopants. Meanwhile, it is noticeable that no significant Cl signal was detected on the annealed sample, which might be due to Cl desorption from the Au(111) surface in the form of Cl_2 gas (see details in Supplementary Figure S1). It is consistent with earlier studies that NaCl islands can

https://doi.org/10.1021/acsnano.3c02819
ACS Nano 2023, 17, 10938−10946

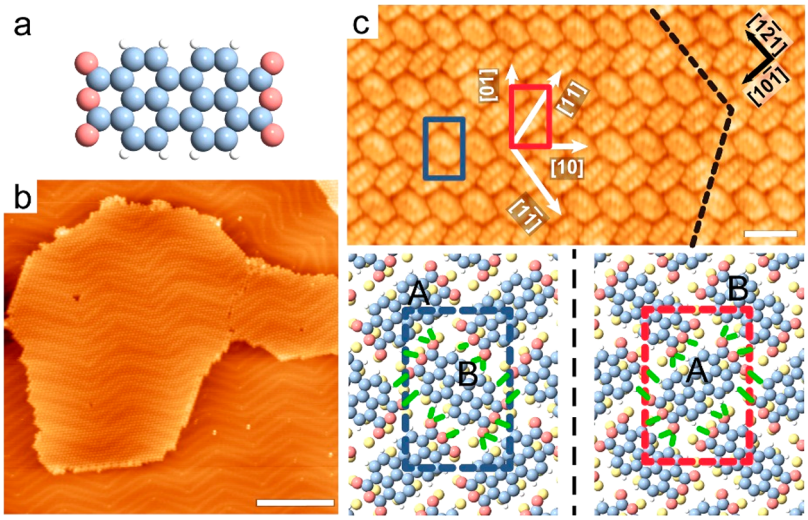

Figure 1. Achiral PTCDA supramolecular network on Au(111). (a) A model of the PTCDA molecule (red balls: oxygen atoms; gray balls: carbon atoms; white balls: hydrogen atoms). (b) The STM image of a well-ordered PTCDA film deposited on the Au(111) surface at RT. (c) A high-resolution STM image of the HB structure of the as-deposited PTCDA film and the structural model in the lower column. The blue and red dashed boxes mark the unit cell with mirror symmetry. White arrows indicate the direction of the HB structure. Black dashed lines indicate the $22 \times \sqrt{3}$ reconstruction orientation of Au(111). Black arrows indicate the direction of the Au(111) surface. Green lines in the lower column indicate the intermolecular hydrogen bonds. Scale bar: (b) 20 nm; (c) 2 nm. Tunneling parameter for (b): Us = −2.3 V, I = 60 pA; (c): Us = −2 V, I = 100 pA.

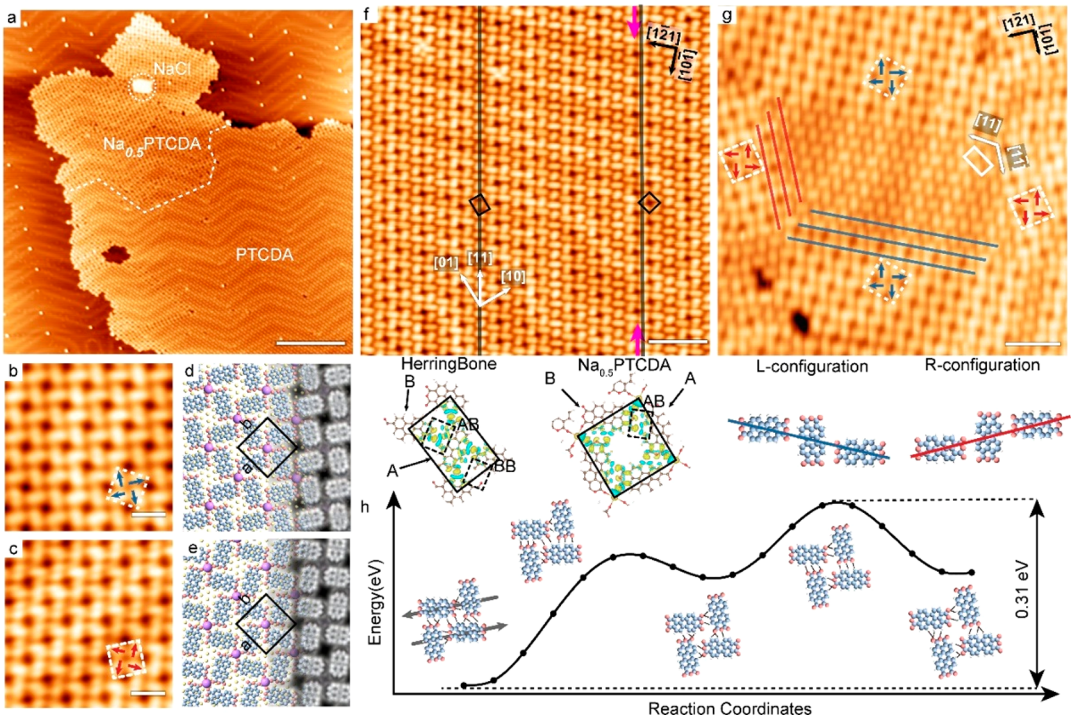

Figure 2. Chirality induction: Na incorporation induced structural phase transition from PTCDA to $Na_{0.5}$PTCDA. (a) STM image of a mixture of PTCDA and predeposited NaCl islands. (b, c) Zoom-in STM images show the left- and right-handed chirality in $Na_{0.5}$PTCDA. (d, e) DFT structural models and simulated STMs of (b) and (c). (f) STM image showing an intermediate state between the HB to $Na_{0.5}$PTCDA phase; white arrows indicate the direction of the HB structure, and pink arrows indicate the row of Na atoms. The direction of the Au surface is marked by black arrows. The lower section is the charge difference at different hydrogen-bonding sites for HB and $Na_{0.5}$PTCDA. (g) STM image of the $Na_{0.5}$PTCDA phase around an HB structure. The solid white box and white arrows mark the unit cell of HB and its direction. Blue and red arrows mark the left- and right-handed $Na_{0.5}$PTCDA, and the lines in corresponding colors indicate the direction of the columns forming them. The lower section is the model for L-configuration and R-configuration of the molecular columns. (h) The energy diagram shows the most optimized pathway of phase transition from HB to $Na_{0.5}$PTCDA. Scale bar: (a) 10 nm, (b, c) 2 nm, (f) 5 nm, (g) 4 nm. Tunneling parameters: Us = −2 V, I = 50 pA.

release Na ions during the annealing process to form coordination networks with organic ligands, and the byproduct molecular Cl is desorbed from the surface.[38] Furthermore, we have also performed a control experiment by using a gas-phase

https://doi.org/10.1021/acsnano.3c02819
ACS Nano 2023, 17, 10938−10946

Na metal source to confirm this porous structure, and the same result is obtained (see Supplementary Figure S2). Thus, we could assign this formed porous structure in Figure 2 as the Na-PTCDA coordination networks.

Next, we probed the structure of the porous Na-PTCDA networks, with an emphasis on their chirality. When the ratio of NaCl to PTCDA coverage is increased to approximately 1:2 and annealed at 320 K for 20 min, the close-packed HB structure totally transformed into the porous phase. Molecules in this pattern have a "windmill" type of unit cell, with each PTCDA molecule shared by two adjacent unit cells and the Na atom located exactly in the rotation center of the windmill, similar to the previously reported $K_{0.5}$PTCDA structure.[42] This "windmill" can rotate either clockwise or counterclockwise, resulting in left-handed or right-handed chiral enantiomers (Figure 2b,c). We find that Na is invisible in most STM images, only showing contrast when the STM tip was tuned to a specific state and under a sample bias at the lowest unoccupied molecular orbital (LUMO) energy level (see Supplementary Figure S3), consistent with previous studies.[43−45] According to the DFT calculations (Figure 2d,e), each PTCDA molecule coordinates to the Na ions via two diagonal carboxyl oxygen atoms, while the other oxygen atoms remain hydrogen bonded to the adjacent PTCDA. The simulated structure, denoted by the chemical formula $Na_{0.5}$PTCDA, has a periodicity of $a = b = 16.05$ Å, which is consistent with the STM-measured periodicity of 15.90 Å (Figure 2b,c). The simulated height of Na ions (3.16 Å) is lower than that of the PTCDA molecules (3.33 Å), which explains why the central Na ions are invisible in most STM images.

To investigate how chirality in the $Na_{0.5}$PTCDA phase is induced from the achiral HB phase, we investigated the intermediate states of structural transformation from PTCDA to $Na_{0.5}$PTCDA. Figure 2f is an STM image of the intermediate state, which can be viewed as a mixture of the PTCDA HB phase and the $Na_{0.5}$PTCDA phase. The HB and $Na_{0.5}$PTCDA units are illustrated by a black rectangle and square, respectively. It is interesting to observe that in both phases the PTCDA molecules are highly oriented along the [11] direction of the PTCDA HB lattice, with alternating A and B molecules (see description in Figure 1c) forming what we called a "molecular column" in this direction, marked by black lines. It suggests that the intermolecular hydrogen bonds along this direction remain intact, and the presence of Na ions, indicated by pink arrows, appears to change the relative position of the adjacent columns. It is noteworthy that depending on the ratio of Na rows and molecular columns, $Na_{0.25}$PTCDA and $Na_{0.16}$PTCDA structures have been imaged as the intermediate phases (see Supplementary Figure S4) between the PTCDA HB phase and the $Na_{0.5}$PTCDA phase.

To rationalize the observation of these molecular columns, we investigated the intermolecular hydrogen bonding of HB and $Na_{0.5}$PTCDA by DFT. As shown in the lower section of Figure 2f, the intermolecular hydrogen bonds linking adjacent molecules of the HB structure can be divided into two groups. One is a pair of parallel hydrogen bonds between two neighboring PTCDA molecules in the same category (AA or BB) along the [10] direction of the HB lattice. Another group is a pair of bifurcated hydrogen bonds and a single hydrogen bond formed by the carboxylic oxygen atoms and anhydride oxygen atoms, respectively, between the alternated adjacent A and B molecules along the [11] and [1$\bar{1}$] directions of the HB lattice.[46] The differential charge density shows that the charge redistribution is significantly more pronounced in the AB molecules than in the AA (or BB) molecules, meaning the AB-type of intermolecular hydrogen bonding is stronger. Next, we investigate the molecular motion during the phase transition by using a simplified model of four molecules and the climbing image nudged elastic band (CI-NEB) method.[47] As shown in Figure 2h, the initial and final states of the system were the PTCDA positions in the HB and $Na_{0.5}$PTCDA structures, respectively. The results showed that the most optimized rearrangement pathway was the relative sliding of the AB molecules along the [11] (or [1$\bar{1}$]) directions, with a potential barrier of 0.31 eV. The stronger hydrogen bonding in the adjacent AB molecules was assigned as the main reason for the sliding-type of molecular rearrangement. Due to steric hindrance, the sliding motion of AB molecules in the compact HB domain is very likely to induce neighboring molecules to move in a similar way, resulting in large-scale collective rearrangement to form PTCDA molecular columns along the [11] (or [1$\bar{1}$]) directions.

The collective molecular rearrangement, which is driven by cooperative hydrogen bonding and steric interactions, is not rare. Similar behaviors have been reported previously, which is termed as the "sergeants and soldiers" principle.[10,48] In addition, we have observed molecular slippage between adjacent PTCDA domains in the pure HB phase, which also preferentially occurs along the [11] or [1$\bar{1}$] directions (see Supplementary Figure S5). This behavior could be induced by thermal fluctuations during growth, and it can also be rationalized as the selective breaking of the AA (or BB) hydrogen bonds and subsequent collective rearrangement of PTCDA molecules.

Based on the above-mentioned model, we can now analyze the chirality induction process in detail. Figure 2g shows an HB domain surrounded by four $Na_{0.5}$PTCDA domains, likely formed by the in-plane incorporation of Na ions released from nearby NaCl domains. The top and bottom domains are left-handed, while the left and right domains are right-handed. The collective rearrangement of PTCDA molecules could be viewed as the relative sliding of adjacent molecular columns. The molecular columns in the HB phase can be assigned in either the [11] or [1$\bar{1}$] directions, indicated by blue and red lines, respectively. The two types of columns are chiral enantiomers with the L- or R-configuration, as they cannot be superimposed via rotations and translations. Apparently, the cooperative-interaction-induced sliding of [11] columns (blue lines) transforms into the left-handed $Na_{0.5}$PTCDA (blue rectangles). In comparison, the sliding of [1$\bar{1}$] columns (red lines) gives rise to the right-handed $Na_{0.5}$PTCDA (see Supplementary Figure S6 for further details). This observation suggests that the direction of Na incorporation is likely to determine the sliding direction of the AB molecules located at the domain edge, which then determines the $Na_{0.5}$PTCDA chirality by inducing the collective rearrangement of PTCDA molecules along the corresponding direction. This implies that if the Na ions were derived from a single direction, homochiral domains would be formed. This is indeed observed in our experiments when only a few PTCDA adsorb around NaCl. As the Na ions are derived from the [10$\bar{1}$] direction of the Au surface to drive collective molecular rearrangement in the [11] direction, a left-handed homochiral domain was observed in Supplementary Figure S7.

https://doi.org/10.1021/acsnano.3c02819
ACS Nano 2023, 17, 10938−10946

To observe whether chirality can be transferred during structural transformation, we supply more NaCl and raise the annealing temperature to promote the further evolution of the self-assembled structure. As shown in Figure 3a, the edge of

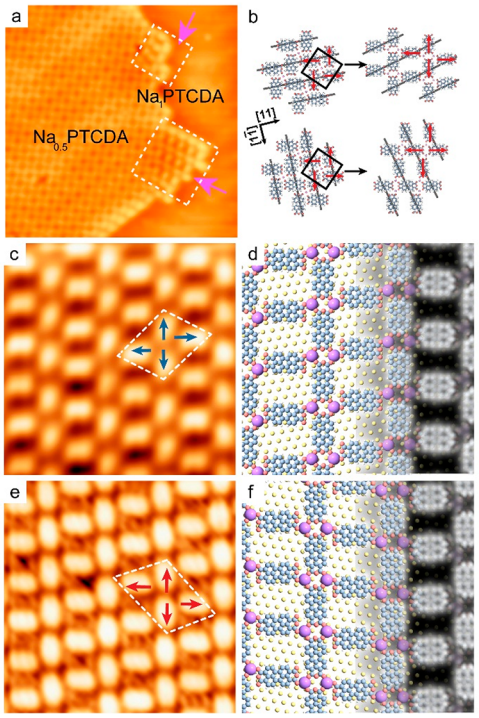

Figure 3. Chirality transfer: Na incorporation induced structural phase transformation from $Na_{0.5}$PTCDA to Na_1PTCDA. (a) STM image of phase transformation of right-handed $Na_{0.5}$PTCDA to right-handed Na_1PTCDA. (b) An illustration of the process shown in (a). The relative slip of the two oriented molecular columns results in forming Na_1PTCDA with the same chirality but a 90-degree rotation in space. (c–f) The STM images, DFT structural models, and simulated STMs for left- and right-handed Na_1PTCDA. Scale bar: (a) 4 nm, (c) and (e) 2 nm. Tunneling parameters: Us = −2 V, *I* = 50 pA.

porous $Na_{0.5}$PTCDA transformed into a ladder-like phase. By further raising the ratio between NaCl and PTCDA to 1:1 and annealing at 380 K for 20 min, the structure is completely transformed into this phase. Similar structures have been observed before in Fe_1PTCDA.[49−51] Depending on the direction of PTCDA, the molecules in this nanostructure are classified as "chain" PTCDA or "rung" PTCDA (Figure 3c,e). Based on DFT calculations, all four carboxyl oxygen atoms in the "chain" PTCDA are engaged in the Na−O coordination. In contrast, only two carboxyl oxygen atoms in the "rung" participate in the production of Na ion coordination bonds, while the remaining two carboxyl oxygen atoms form hydrogen bonds with the hydrogen donor of the "chain" PTCDA. This ladder-like motif, denoted by the chemical formula of Na_1PTCDA, has the basic cell size of a = 15.26 Å, b = 25.20 Å, and an angle of 73° between them (Figure 3d,f), which is consistent with our STM-measured dimensions.

This phase also has left-handed and right-handed chiral enantiomers, as shown in Figure 3c,e. Interestingly, in Figure 3a, the right-handed chiral $Na_{0.5}$PTCDA is converted to two right-handed chiral Na_1PTCDA domains with a 90-degree rotation in space. Here we assume the cooperative hydrogen bonding and steric interactions still govern the molecular rearrangement, but now with AB molecules held by only two bifurcated hydrogen bonds. Based on this assumption, we assign molecular columns in the $Na_{0.5}$PTCDA structure along the [11] and [1$\bar{1}$] directions (marked by gray lines in Figure 3b). Due to the 4-fold rotational symmetry of $Na_{0.5}$PTCDA, a 90-degree rotation brings the [11] orientation columns into coincidence with the [1$\bar{1}$] orientation columns, resulting in all columns being classified as the R-configuration. The Na_1PTCDA formed by the columns in the [11] direction sliding against each other also coincides with the Na_1PTCDA formed by the columns in the [1$\bar{1}$] orientation after 90 deg of rotation. Hence, the right-handed chiral $Na_{0.5}$PTCDA only transforms into the right-handed chiral Na_1PTCDA, and the left-handed chiral $Na_{0.5}$PTCDA transforms only into the left-handed chiral Na_1PTCDA, regardless of the sliding direction of the molecular columns. This evolution implies that for $Na_{0.5}$PTCDA the chirality will be transferred to Na_1PTCDA regardless of the direction of Na incorporation.

Finally, we observed the termination of chirality transfer from Na_1PTCDA to Na_2PTCDA as shown in Figure 4a. The

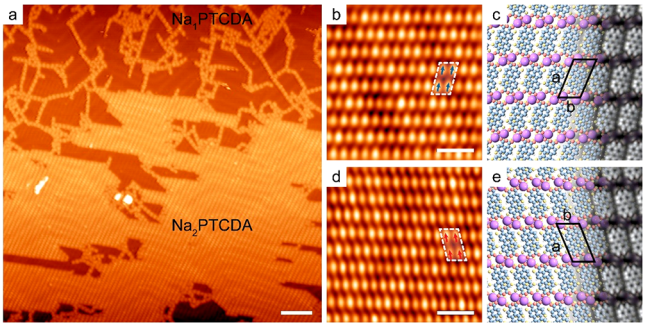

Figure 4. Disruption of chirality transfer: formation of the Na_2PTCDA phase on the Au(111) surface. (a) STM image of phase transformation from Na_1PTCDA to Na_2PTCDA mediated by one-dimensional achiral Na_2PTCDA chains. (b–e) The STM images, DFT structural models, and simulated STMs for left- and right-handed Na_2PTCDA. Scale bar: (a) 10 nm, (b, d) 2 nm. Tunneling parameters: Us = −2 V,*I* = 50 pA.

Na_2PTCDA network with the highest doping ratio of Na ions is available at a 2:1 ratio of NaCl and PTCDA, coverages, and then is annealed at 480 K for 20 min. As shown in Figure 4b,d, the STM image shows a close-packed structure in which all molecules form rows by aligning side-by-side, similar to the previously reported K_2PTCDA/Ag(111).[27,28] In the DFT model (Figure 4c,e), all oxygen atoms are coordinated to the Na ions, resulting in two double-coordinated carboxyl oxygen atoms and two single-coordinated carboxyl oxygen atoms per molecule. Each unit cell consists of one PTCDA molecule and two Na ions, with the cell dimensions of a = 15.26 Å, b = 8.65 Å, and a separation angle of 79°, which is consistent with the STM-measured periodicity of a = 16.05 Å, b = 8.92 Å, and a separation angle of 80°. The molecule's short axis rotates relative to the row direction (lattice vector b) owing to the different coordination numbers of the two carboxyl oxygen atoms on either side of the molecule's short axis. The direction of the rotation, either clockwise or counterclockwise, defines the handedness of an enantiomer. In the STM image (Figure 4a), it is evident that one-dimensional achiral Na_2PTCDA chains are observed instead of close-packed domains,[49] implying that the PTCDA molecules no longer rearrange

https://doi.org/10.1021/acsnano.3c02819
ACS Nano 2023, 17, 10938−10946

collectively during the phase transition to the Na_2PTCDA phase. This is not surprising since all the intermolecular hydrogen bonds, which hold the AB molecules in position, are now completely replaced by Na−O coordination bonds. Therefore, the chirality of the Na_2PTCDA domains arises randomly and cannot be inherited from that of the Na_1PTCDA structure.

CONCLUSIONS

The chirality induction and transfer mechanism underlying metal−organic self-assembly, which are crucial for developing enantioselective assembly strategies, are often difficult to comprehend due to the difficulty in observing the fast assembly processes. Previous studies on the self-assembled PTCDA structure on Au(111) using gaseous metal Na sources have resulted in the spontaneous formation of all Na-PTCDA networks, making it difficult to observe the intermediate states during structural evolution (Supplementary Figure S1). In our work, we used NaCl as the solid-state Na source and controlled the thermal annealing conditions to precisely regulate the rate and stage of structural transformation from the achiral PTCDA structure to the chiral Na-PTCDA coordination networks. With the increased surface Na ion concentrations, chiral $Na_{0.5}$PTCDA, Na_1PTCDA, and Na_2PTCDA structures have been obtained, similar to the $K_{0.5}$PTCDA, Fe_1PTCDA, and K_2PTCDA structures reported previously.[27,28,42,49−51] These ratios are also confirmed by scanning tunneling spectroscopy in terms of continuous electric doping, as shown in Supplementary Figure S8.

Our results showed that early-stage Na ion incorporation only partially breaks the intermolecular hydrogen bonds in the self-assembled HB structure of PTCDA molecules. Subsequently, due to the cooperative hydrogen-bonding and steric interactions among neighboring molecules, a sliding-type of collective rearrangement along the [11] or $[1\bar{1}]$ direction will occur, resulting in the formation of highly oriented molecular columns in the corresponding direction. This collective rearrangement behavior can be regulated by the direction of Na ion incorporation and gave rise to the chirality induction and transfer processes. Our observations also revealed that the chirality transfer was disrupted at high surface Na ion concentrations, as intermolecular hydrogen bonds that held the collective molecular rearrangement were completely replaced by Na coordination bonds.

These findings demonstrate that the comprehension of introducing and transferring chirality by using nonchiral precursors such as Na atoms and PTCDA may lead to strategies capable of producing large-scale homochiral Na-PTCDA networks. For example, anisotropic metal substrates such as Au(100) or Au(110) could be used to control the Na ion incorporation from a single surface direction, triggering the structural transformation of self-assembled PTCDA structures in an enantioselective manner. Furthermore, our DFT simulation reveals that this kind of Na-PTCDA network exhibits chirality-dependent light−matter interactions (Supplementary Figure S9). Such tunable chiral networks have the potential to serve as chiral electronic or optoelectronic materials with a wide range of applications, including the filtration of spin currents and the selective emission of light with different polarizations.

METHODS

STM Measurement. The experiments were performed in an ultrahigh-vacuum (UHV) system equipped with a low-temperature STM (Unisoku 1400) at a base pressure of 1×10^{-10} Torr. The single-crystal Au(111) surface was prepared by several cycles of 1.5 keV Ar^+ sputtering followed by annealing to 850 K, resulting in clean and flat terraces separated by monatomic steps. Tungsten tips were electrochemically etched and cleaned by an e-beam bombardment. After the system was thoroughly degassed, the PTCDA molecules and NaCl were sublimated respectively from a multisource miniature Knudsen cell (K cell) onto the Au(111) surface followed by stepwise annealing. To conduct a control experiment with a different source of Na, a direct incorporation of Na was carried out by cracking a commercial Na distributor source (SAES Getters) while applying a DC current of I = 5.0 A. STM imaging and scanning tunneling spectroscopy (STS) measurements were performed at T = 78 K. dI/dV spectra on the Au(111) substrate were used as an STS reference for tip calibration. STM/STS data were analyzed and rendered using the WSxM software.[52]

XPS Measurement. XPS analysis was performed with monochromatic Al Kα emission (1486.6 eV) using an XM-1200 X-ray source (SCIENTA OMICRON GmbH) in a UHV chamber with a base pressure of 5×10^{-10} mbar. The photoelectrons were analyzed by a SCIENTA OMICRON DA30 hemispherical analyzer (SCIENTA OMICRON GmbH), working with a 200 eV pass energy to accommodate weak signals. Following STM measurements, the samples were promptly transferred to the XPS system. All XPS measurements were performed at room temperature, and binding energy was calibrated using the Au 4f reference (Au $4f_{7/2}$ = 84.0 eV). Curve fitting was accomplished using an integrated Shirley-type background and combined Gaussian−Lorentzian line shape with the Igor Pro program. The analyzed samples had only a minimal amount of carbon contamination.

DFT Calculations. The DFT calculations were performed by applying the repeated slab approach using the Vienna Ab Initio Simulation Package (VASP) code.[53] The projector augmented wave method was used to describe the interaction between ions and electrons, and the Perdew−Burke−Ernzerh of the generalized gradient approximation exchange−correlation functional was employed.[54] van der Waals corrections to the PBE were also included using the Tkatchenko−Scheffler custom method.[55] Plane waves were used as a basis set with an energy cutoff of 400 eV. The Brillouin zone was sampled by 3 × 3 × 1, 5 × 5 × 1, 3 × 3 × 1, and 3 × 5 × 1 Monkhorst−Pack k-point sampling[56] for structural optimizations of PTCDA/Au(111), $Na_{0.5}$PTCDA/Au(111), Na_1PTCDA/Au(111), and Na_2PTCDA/Au(111), respectively. The Au(111) surface was sampled with a slab model consisting of three layers of Au atoms. The geometry of PTCDA, Na atoms, and the top two layers of Au atoms within the unit cell was allowed to structurally relax in three dimensions until the atomic force was smaller than 0.01 eV/Å. The atomic structures were relaxed using the conjugate gradient algorithm scheme as implemented in VASP until the energy changes were $\leq 1 \times 10^{-4}$ eV. The STM images were simulated by integrating the local density of states between the Fermi energy (EF) and the Fermi energy plus the applied tunneling bias (VT) following the Tersoff−Hamann approach.[57] In order to analyze the involved hydrogen bonds, we also performed the charge density difference due to the intermolecular interaction following Harry Mönig's recipe.[46] Here, the formula is defined as $\Delta\rho = \rho_{tot} - \rho_{molec}$, where ρ_{tot} is the total charge density and ρ_{molec} is the charge density of the individual molecules. To study the transition behaviors from PTCDA to $Na_{0.5}$PTCDA, the energy barrier ΔE along the transition path has been calculated using the CI-NEB method.[47] To study the electronic circular dichroism spectra of Na-PTCDA nanostructures, time-dependent DFT was employed,[58] using the B3LYP hybrid functional.[59]

https://doi.org/10.1021/acsnano.3c02819
ACS Nano 2023, 17, 10938−10946

ASSOCIATED CONTENT

Supporting Information

The Supporting Information is available free of charge at https://pubs.acs.org/doi/10.1021/acsnano.3c02819.

XPS results of NaCl/Au(111) and $Na_{0.5}$PTCDA/Au(111); an STM image showing the result of a control experiment utilizing Na getter sources to prepare Na-PTCDA complexes; STM images at the special tip state; diagrams showing formation processes of $Na_{0.16}$PTCDA, $Na_{0.25}$PTCDA, and $Na_{0.5}$PTCDA; molecular slippage between adjacent PTCDA domains in the HB phase; a diagram of a molecular column; an STM image showing molecular columns rearranged into the left-handed $Na_{0.5}$PTCDA; STS spectra measured on different structures of Na-PTCDA complexes; electronic circular dichroism spectra of Na-PTCDA complexes (PDF)

AUTHOR INFORMATION

Corresponding Authors

Liang Cao − *Anhui Key Laboratory of Condensed Matter Physics at Extreme Conditions, High Magnetic Field Laboratory, HFIPS, Chinese Academy of Sciences, Hefei 230031, People's Republic of China;* orcid.org/0000-0001-7453-7060; Email: lcao@hmfl.ac.cn

Hai Xu − *Changchun Institute of Optics, Fine Mechanics & Physics (CIOMP), Chinese Academy of Sciences, Changchun 130033, People's Republic of China; University of Chinese Academy of Sciences, Chinese Academy of Sciences, Beijing 100049, People's Republic of China;* orcid.org/0000-0002-4047-7087; Email: xuhai@ciomp.ac.cn

Authors

Zhewen Liang − *Changchun Institute of Optics, Fine Mechanics & Physics (CIOMP), Chinese Academy of Sciences, Changchun 130033, People's Republic of China; University of Chinese Academy of Sciences, Chinese Academy of Sciences, Beijing 100049, People's Republic of China;* orcid.org/0009-0002-6353-3528

Shiru Wu − *Key Laboratory of Flexible Electronics (KLOFE) & Institute of Advanced Materials (IAM), Nanjing Tech University (Nanjing Tech), Nanjing 211816, People's Republic of China*

Jiamin Wang − *Changchun Institute of Optics, Fine Mechanics & Physics (CIOMP), Chinese Academy of Sciences, Changchun 130033, People's Republic of China; University of Chinese Academy of Sciences, Chinese Academy of Sciences, Beijing 100049, People's Republic of China*

Yifan Qin − *Changchun Institute of Optics, Fine Mechanics & Physics (CIOMP), Chinese Academy of Sciences, Changchun 130033, People's Republic of China; University of Chinese Academy of Sciences, Chinese Academy of Sciences, Beijing 100049, People's Republic of China*

Fang Cheng − *State Key Laboratory for Organic Electronics and Information Displays & Jiangsu Key Laboratory for Biosensors, Institute of Advanced Materials (IAM), Jiangsu National Synergetic Innovation Center for Advanced Materials (SICAM), Nanjing University of Posts and Telecommunications, Nanjing 210023, People's Republic of China;* orcid.org/0000-0003-1645-4237

Complete contact information is available at: https://pubs.acs.org/10.1021/acsnano.3c02819

Author Contributions

The manuscript was written through contributions of all authors. All authors have given approval to the final version of the manuscript.

Notes

The authors declare no competing financial interest.

ACKNOWLEDGMENTS

This work was supported by National Natural Science Foundation of China (11727902, 12074372, 12074385, 21902079), the Natural Science Foundation of Jiangsu Province of China (BK20190724), and Open Project of the State Key Laboratory of Luminescence and Applications (SKLA-2020-08). We thank Prof. Yang Bao and Prof. Jiaxu Yan for fruitful discussions and proofreading of the manuscript.

REFERENCES

(1) Aoki, R.; Toyoda, R.; Kögel, J. F.; Sakamoto, R.; Kumar, J.; Kitagawa, Y.; Harano, K.; Kawai, T.; Nishihara, H. Bis(Dipyrrinato)-Zinc(II) Complex Chiroptical Wires: Exfoliation into Single Strands and Intensification of Circularly Polarized Luminescence. *J. Am. Chem. Soc.* **2017**, *139* (45), 16024−16027.

(2) Naaman, R.; Paltiel, Y.; Waldeck, D. H. Chiral Molecules and the Electron Spin. *Nat. Rev. Chem.* **2019**, *3* (4), 250−260.

(3) Cinchetti, M.; Neuschwander, S.; Fischer, A.; Ruffing, A.; Mathias, S.; Wüstenberg, J.-P.; Aeschlimann, M. Tailoring the Spin Functionality of a Hybrid Metal-Organic Interface by Means of Alkali-Metal Doping. *Phys. Rev. Lett.* **2010**, *104* (21), 217602.

(4) Naaman, R.; Waldeck, D. H. Chiral-Induced Spin Selectivity Effect. *J. Phys. Chem. Lett.* **2012**, *3* (16), 2178−2187.

(5) Ernst, K.-H. Molecular Chirality at Surfaces. *Phys. Status Solidi B* **2012**, *249* (11), 2057−2088.

(6) Fang, Y.; Ghijsens, E.; Ivasenko, O.; Cao, H.; Noguchi, A.; Mali, K. S.; Tahara, K.; Tobe, Y.; De Feyter, S. Dynamic Control over Supramolecular Handedness by Selecting Chiral Induction Pathways at the Solution−Solid Interface. *Nat. Chem.* **2016**, *8* (7), 711−717.

(7) Xu, Y.; Duan, J.-J.; Yi, Z.-Y.; Zhang, K.-X.; Chen, T.; Wang, D. Chirality of Molecular Nanostructures on Surfaces via Molecular Assembly and Reaction: Manifestation and Control. *Surf. Sci. Rep.* **2021**, *76* (3), 100531.

(8) Zaera, F. Chirality in Adsorption on Solid Surfaces. *Chem. Soc. Rev.* **2017**, *46* (23), 7374−7398.

(9) Telychko, M.; Li, G.; Mutombo, P.; Soler-Polo, D.; Peng, X.; Su, J.; Song, S.; Koh, M. J.; Edmonds, M.; Jelínek, P.; Wu, J.; Lu, J. Ultrahigh-Yield on-Surface Synthesis and Assembly of Circum-coronene into a Chiral Electronic Kagome-Honeycomb Lattice. *Sci. Adv.* **2021**, *7* (3), eabf0269.

(10) Tahara, K.; Yamaga, H.; Ghijsens, E.; Inukai, K.; Adisoejoso, J.; Blunt, M. O.; De Feyter, S.; Tobe, Y. Control and Induction of Surface-Confined Homochiral Porous Molecular Networks. *Nat. Chem.* **2011**, *3* (9), 714−719.

(11) Shchyrba, A.; Nguyen, M.-T.; Wäckerlin, C.; Martens, S.; Nowakowska, S.; Ivas, T.; Roose, J.; Nijs, T.; Boz, S.; Schär, M.; Stöhr, M.; Pignedoli, C. A.; Thilgen, C.; Diederich, F.; Passerone, D.; Jung, T. A. Chirality Transfer in 1D Self-Assemblies: Influence of H-Bonding vs Metal Coordination between Dicyano[7]Helicene Enantiomers. *J. Am. Chem. Soc.* **2013**, *135* (41), 15270−15273.

(12) Chen, T.; Wang, D.; Wan, L.-J. Two-Dimensional Chiral Molecular Assembly on Solid Surfaces: Formation and Regulation. *Natl. Sci. Rev.* **2015**, *2* (2), 205−216.

(13) Wang, T.; Lv, H.; Huang, J.; Shan, H.; Feng, L.; Mao, Y.; Wang, J.; Zhang, W.; Han, D.; Xu, Q.; Du, P.; Zhao, A.; Wu, X.; Tait, S. L.; Zhu, J. Reaction Selectivity of Homochiral versus Heterochiral Intermolecular Reactions of Prochiral Terminal Alkynes on Surfaces. *Nat. Commun.* **2019**, *10* (1), 4122.

(14) Chen, Y.; Chen, C.; Ding, P.; Shi, G.; Sun, Y.; Kantorovich, L. N.; Besenbacher, F.; Yu, M. Molecular Recognition and Homochir-

ality Preservation of Guanine Tetrads in the Presence of Melamine. *Nano Res.* **2020**, *13* (9), 2427−2430.
(15) Chen, Z.; Lin, T.; Li, H.; Sun, M.; Su, C.; Huang, B.; Loh, K. P. Chiral Self-Assembly of Terminal Alkyne and Selenium Clusters Organic-Inorganic Hybrid. *Nano Res.* **2022**, *15* (3), 2741−2745.
(16) Stepanow, S.; Ohmann, R.; Leroy, F.; Lin, N.; Strunskus, T.; Wöll, C.; Kern, K. Rational Design of Two-Dimensional Nanoscale Networks by Electrostatic Interactions at Surfaces. *ACS Nano* **2010**, *4* (4), 1813−1820.
(17) Han, D.; Wang, T.; Huang, J.; Li, X.; Zeng, Z.; Zhu, J. Chiral Nanoporous Networks Featuring Various Chiral Vertices from an Achiral Molecule on Ag(100). *Nano Res.* **2022**, *15* (4), 3753−3762.
(18) Shi, M.-X.; Xu, J.; Sun, K.; Tao, M.-L.; Yang, J.-Y.; Yang, D.-X.; Wang, Z.-L.; Li, Z.; Wang, J.-Z.; Xue, Q.-K.; Meng, S. Simultaneous Switching of Supramolecular Chirality and Organizational Chirality Driven by Coulomb Expansion. *Nano Res.* **2022**, *15* (6), 5316−5321.
(19) Xie, L.; Ding, Y.; Li, D.; Zhang, C.; Wu, Y.; Sun, L.; Liu, M.; Qiu, X.; Xu, W. Local Chiral Inversion of Thymine Dimers by Manipulating Single Water Molecules. *J. Am. Chem. Soc.* **2022**, *144* (11), 5023−5028.
(20) Chen, W.; Li, H.; Huang, H.; Fu, Y.; Zhang, H. L.; Ma, J.; Wee, A. T. S. Two-Dimensional Pentacene:3,4,9,10-Perylenetetracarboxylic Dianhydride Supramolecular Chiral Networks on Ag(111). *J. Am. Chem. Soc.* **2008**, *130* (37), 12285−12289.
(21) Telychko, M.; Su, J.; Gallardo, A.; Gu, Y.; Mendieta-Moreno, J. I.; Qi, D.; Tadich, A.; Song, S.; Lyu, P.; Qiu, Z.; Fang, H.; Koh, M. J.; Wu, J.; Jelínek, P.; Lu, J. Strain-Induced Isomerization in One-Dimensional Metal−Organic Chains. *Angew. Chem.* **2019**, *131* (51), 18764−18770.
(22) Messina, P.; Dmitriev, A.; Lin, N.; Spillmann, H.; Abel, M.; Barth, J. V.; Kern, K. Direct Observation of Chiral Metal-Organic Complexes Assembled on a Cu(100) Surface. *J. Am. Chem. Soc.* **2002**, *124* (47), 14000−14001.
(23) Spillmann, H.; Dmitriev, A.; Lin, N.; Messina, P.; Barth, J. V.; Kern, K. Hierarchical Assembly of Two-Dimensional Homochiral Nanocavity Arrays. *J. Am. Chem. Soc.* **2003**, *125* (35), 10725−10728.
(24) Xiao, W.; Feng, X.; Ruffieux, P.; Gröning, O.; Müllen, K.; Fasel, R. Self-Assembly of Chiral Molecular Honeycomb Networks on Au(111). *J. Am. Chem. Soc.* **2008**, *130* (28), 8910−8912.
(25) Shu, C.-H.; He, Y.; Zhang, R.-X.; Chen, J.-L.; Wang, A.; Liu, P.-N. Atomic-Scale Visualization of Stepwise Growth Mechanism of Metal-Alkynyl Networks on Surfaces. *J. Am. Chem. Soc.* **2020**, *142* (39), 16579−16586.
(26) Chen, T.; Yang, W.-H.; Wang, D.; Wan, L.-J. Globally Homochiral Assembly of Two-Dimensional Molecular Networks Triggered by Co-Absorbers. *Nat. Commun.* **2013**, *4* (1), 1389.
(27) Zwick, C.; Baby, A.; Gruenewald, M.; Verwüster, E.; Hofmann, O. T.; Forker, R.; Fratesi, G.; Brivio, G. P.; Zojer, E.; Fritz, T. Complex Stoichiometry-Dependent Reordering of 3,4,9,10-Perylene-tetracarboxylic Dianhydride on Ag(111) upon K Intercalation. *ACS Nano* **2016**, *10* (2), 2365−2374.
(28) Baby, A.; Gruenewald, M.; Zwick, C.; Otto, F.; Forker, R.; van Straaten, G.; Franke, M.; Stadtmüller, B.; Kumpf, C.; Brivio, G. P.; Fratesi, G.; Fritz, T.; Zojer, E. Fully Atomistic Understanding of the Electronic and Optical Properties of a Prototypical Doped Charge-Transfer Interface. *ACS Nano* **2017**, *11* (10), 10495−10508.
(29) Heimer, K.; Wuesten, J.; Lach, S.; Ziegler, Ch. Interaction of Alkali Metals with Perylene-3,4,9,10-Tetracarboxylic-Dianhydride Thin Films Studied by IR Spectroscopy. *J. Chem. Phys.* **2007**, *126* (16), 164709.
(30) Fuentes, G. G.; Knupfer, M. Electronic Structure and Work Function of Potassium-Doped PTCDA Thin Films. *Appl. Phys. A: Mater. Sci. Process.* **2006**, *84* (3), 329−333.
(31) Wüsten, J.; Heimer, K.; Lach, S.; Ziegler, Ch. Alkali Metals in Perylene-3,4,9,10-Tetracarboxylicdianhydride Thin Films. *J. Appl. Phys.* **2007**, *102* (2), No. 023708.
(32) Zazza, C.; Meloni, S.; Palma, A.; Knupfer, M.; Fuentes, G. G.; Car, R. Quasi-One-Dimensional K-O Chain in PTCDA Thin Films: Evidence from First-Principles Calculations. *Phys. Rev. Lett.* **2007**, *98* (4), No. 046401.
(33) Dienel, T.; Krause, A.; Alle, R.; Forker, R.; Meerholz, K.; Fritz, T. Alkali Metal Doped Organic Molecules on Insulators: Charge Impact on the Optical Properties. *Adv. Mater.* **2010**, *22* (36), 4064−4070.
(34) Zhou, G.; Miao, Y.-E.; Wei, Z.; Mo, L.; Lai, F.; Wu, Y.; Ma, J.; Liu, T. Bioinspired Micro/Nanofluidic Ion Transport Channels for Organic Cathodes in High-Rate and Ultrastable Lithium/Sodium-Ion Batteries. *Adv. Funct. Mater.* **2018**, *28* (52), 1804629.
(35) Lian, X.; Ma, Z.; Zhang, Z.; Yang, J.; Liu, Y.; Gu, C.; Guo, R.; Wang, Y.; Ye, X.; Sun, S.; Zheng, Y.; Ding, H.; Hu, J.; Cao, X.; Mao, H.; Zhu, J.; Li, S.; Chen, W. Alkali Metal Storage Mechanism in Organic Semiconductor of Perylene-3,4,9,10-Tetracarboxylicdianhydride. *Appl. Surf. Sci.* **2020**, *524*, 146396.
(36) Wüsten, J.; Berger, S.; Salomo, M.; Mönnich, A.; Bauer, M.; Lach, S.; Aeschlimann, M.; Ziegler, Ch. Hot-Electron Dynamics in Thin Films of Sodium-Doped Perylene-3,4,9,10-Tetracarboxylic Dianhydride. *Phys. Rev. B* **2008**, *78* (19), 195326.
(37) Skomski, D.; Abb, S.; Tait, S. L. Robust Surface Nano-Architecture by Alkali−Carboxylate Ionic Bonding. *J. Am. Chem. Soc.* **2012**, *134* (34), 14165−14171.
(38) Hieulle, J.; Peyrot, D.; Jiang, Z.; Silly, F. Engineering Two-Dimensional Hybrid NaCl−Organic Coordinated Nanoarchitectures on Metal Surfaces. *Chem. Commun.* **2015**, *51* (67), 13162−13165.
(39) Temirov, R.; Soubatch, S.; Luican, A.; Tautz, F. S. Free-Electron-like Dispersion in an Organic Monolayer Film on a Metal Substrate. *Nature* **2006**, *444* (7117), 350−353.
(40) Schmitz-Hübsch, T.; Fritz, T.; Sellam, F.; Staub, R.; Leo, K. Epitaxial Growth of 3,4,9,10-Perylene-Tetracarboxylic-Dianhydride on Au(111): A STM and RHEED Study. *Phys. Rev. B* **1997**, *55* (12), 7972−7976.
(41) Rohlfing, M.; Temirov, R.; Tautz, F. S. Adsorption Structure and Scanning Tunneling Data of a Prototype Organic-Inorganic Interface: PTCDA on Ag(111). *Phys. Rev. B* **2007**, *76* (11), 115421.
(42) Weiss, C.; Wagner, C.; Temirov, R.; Tautz, F. S. Direct Imaging of Intermolecular Bonds in Scanning Tunneling Microscopy. *J. Am. Chem. Soc.* **2010**, *132* (34), 11864−11865.
(43) Chen, C.; Ding, P.; Mura, M.; Chen, Y.; Sun, Y.; Kantorovich, L. N.; Gersen, H.; Besenbacher, F.; Yu, M. Formation of Hypoxanthine Tetrad by Reaction with Sodium Chloride: From Planar to Stereo. *Angew. Chem., Int. Ed.* **2018**, *57* (49), 16015−16019.
(44) Blowey, P. J.; Sohail, B.; Rochford, L. A.; Lafosse, T.; Duncan, D. A.; Ryan, P. T. P.; Warr, D. A.; Lee, T.-L.; Costantini, G.; Maurer, R. J.; Woodruff, D. P. Alkali Doping Leads to Charge-Transfer Salt Formation in a Two-Dimensional Metal−Organic Framework. *ACS Nano* **2020**, *14* (6), 7475−7483.
(45) Chen, C.; Sang, H.; Ding, P.; Sun, Y.; Mura, M.; Hu, Y.; Kantorovich, L. N.; Besenbacher, F.; Yu, M. Xanthine Quartets on Au(111). *J. Am. Chem. Soc.* **2018**, *140* (1), 54−57.
(46) Mönig, H.; Amirjalayer, S.; Timmer, A.; Hu, Z.; Liu, L.; Díaz Arado, O.; Cnudde, M.; Strassert, C. A.; Ji, W.; Rohlfing, M.; Fuchs, H. Quantitative Assessment of Intermolecular Interactions by Atomic Force Microscopy Imaging Using Copper Oxide Tips. *Nat. Nanotechnol.* **2018**, *13* (5), 371−375.
(47) Henkelman, G.; Uberuaga, B. P.; Jónsson, H. A. Climbing Image Nudged Elastic Band Method for Finding Saddle Points and Minimum Energy Paths. *J. Chem. Phys.* **2000**, *113* (22), 9901−9904.
(48) Green, M. M.; Reidy, M. P.; Johnson, R. D.; Darling, G.; O'Leary, D. J.; Willson, G. Macromolecular Stereochemistry: The out-of-Proportion Influence of Optically Active Comonomers on the Conformational Characteristics of Polyisocyanates. The Sergeants and Soldiers Experiment. *J. Am. Chem. Soc.* **1989**, *111* (16), 6452−6454.
(49) Méndez, J.; Caillard, R.; Otero, G.; Nicoara, N.; Martín-Gago, J. A. Nanostructured Organic Material: From Molecular Chains to Organic Nanodots. *Adv. Mater.* **2006**, *18* (15), 2048−2052.
(50) Yang, H.-H.; Chu, Y.-H.; Lu, C.-I.; Yang, T.-H.; Yang, K.-J.; Kaun, C.-C.; Hoffmann, G.; Lin, M.-T. Digitized Charge Transfer

https://doi.org/10.1021/acsnano.3c02819
ACS Nano 2023, 17, 10938−10946

Magnitude Determined by Metal−Organic Coordination Number. *ACS Nano* **2013**, *7* (3), 2814−2819.
(51) Álvarez, L.; Peláez, S.; Caillard, R.; Serena, P. A.; Martín-Gago, J. A.; Méndez, J. Metal-Organic Extended 2D Structures: Fe-PTCDA on Au(111). *Nanotechnology* **2010**, *21* (30), 305703.
(52) Horcas, I.; Fernández, R.; Gómez-Rodríguez, J. M.; Colchero, J.; Gómez-Herrero, J.; Baro, A. M. WSXM: A Software for Scanning Probe Microscopy and a Tool for Nanotechnology. *Rev. Sci. Instrum.* **2007**, *78* (1), No. 013705.
(53) Kresse, G.; Furthmüller, J. Efficient Iterative Schemes for Ab Initio Total-Energy Calculations Using a Plane-Wave Basis Set. *Phys. Rev. B* **1996**, *54* (16), 11169−11186.
(54) Perdew, J. P.; Burke, K.; Ernzerhof, M. Generalized Gradient Approximation Made Simple. *Phys. Rev. Lett.* **1996**, *77* (18), 3865−3868.
(55) Ruiz, V. G.; Liu, W.; Zojer, E.; Scheffler, M.; Tkatchenko, A. Density-Functional Theory with Screened van Der Waals Interactions for the Modeling of Hybrid Inorganic-Organic Systems. *Phys. Rev. Lett.* **2012**, *108* (14), 146103.
(56) Monkhorst, H. J.; Pack, J. D. Special Points for Brillouin-Zone Integrations. *Phys. Rev. B* **1976**, *13* (12), 5188−5192.
(57) Tersoff, J.; Hamann, D. R. Theory of the Scanning Tunneling Microscope. *Phys. Rev. B* **1985**, *31* (2), 805−813.
(58) Autschbach, J.; Ziegler, T. Calculating molecular electric and magnetic properties from time-dependent density functional response theory. *J. Chem. Phys.* **2002**, *116*, 891−896.
(59) Becke, A. D. Density-Functional Thermochemistry. III., The Role of Exact Exchange. *J. Chem. Phys.* **1993**, *98*, 5648−5652.

https://doi.org/10.1021/acsnano.3c02819
ACS Nano 2023, 17, 10938−10946